J. P. Kastillo[1] / J. Martínez-Gómez[1,2] / S. P. Villacis[1] / A. J. Riofrio[1]

Thermal Natural Convection Analysis of Olive Oil in Different Cookware Materials for Induction Stoves

[1] Instituto Nacional de Eficiencia Energética y Energías Renovables (INER), Iñaquito N35-37 y Juan Pablo Sanz, Edificio Colegio de Economistas de Pichincha, 3er piso., Quito, Ecuador, E-mail: javier.martinez@iner.gob.ec

[2] Facultad de Ingeniería y Ciencias Aplicadas, Universidad Internacional SEK, 170302 Quito, Ecuador E-mail: javier.martinez@uisek.edu.ec

Abstract:
This manuscript describes the analysis of temperature and the distribution of natural convection flow of three different cookware materials composed of stainless steel, aluminum and enameled iron, when heating olive oil. A Computational Fluid Dynamic (CFD) software, called COMSOL Multiphysics©, has been used to analyze the heat transfer process for this study. In addition, a thermographic camera and a particle tracer were employed to compare the measurements of temperature, heat transfer and flow velocity, obtained from the CFD analysis. The results demonstrated that the enameled iron was the best choice of cookware material for induction stoves, as with the increment of oil temperature, this material had the biggest contrails and oil velocity convection flow in the center of the cookware.

Keywords: induction heating, computational fluid dynamic, heat transfer analysis, olive oil, cookware

DOI: 10.1515/ijfe-2016-0065

1 Introduction

The Induction Heating (IH) principle in an induction stove works due to the alternating current flow generated in the coil, which produces an alternating magnetic field that is inducted on the ferromagnetic bottom of the cookware [1–3]. The increase of the induction stoves demand at a household level, is because induction stoves have several advantages in comparison to conventional liquefied petroleum gas (LPG) based stoves and elec-tric coil stoves [1–3]. The most important advantages are: i) energy efficiency, due to the reduction of heating losses at households by the induced magnetic field in cookware; ii) enhanced safety, there is no flame during cooking; iii) no waste of energy when cookware is removed from the hob; iv) automatic cut–off function in case of overheating; v) no emission of harmful fuel gasses; vi) easy to clean [1–3].

The use of induction stoves was promoted in Ecuador. The Ecuadorian government is developing a world pioneer policy called "The national efficient cooking plan", which aims that 3 million LPG-based stoves migrate to induction stoves [4, 5]. In this way, the cookware manufacturing industry needs a study, where different cookware materials are examined in terms of better performance and results during heating a fluid and energy efficiency when using induction stoves.

In food engineering, the Computational Fluid Dynamic (CFD) is applied to the numerical solution of the Navier-Stokes Transport Equations, to show the results of the conservation of mass and momentum, energy and state equations given by the initial and boundary conditions of the computational domain [6–8]. CFD employed to improve the quality and safety of the different food processing operations such as mixing, heating, drying, cooking, freezing, pasteurization and sterilization relying on fluid flow [6–11]. The most significant studies related to CFD in the food industry were summarized as follows. The thermal sterilization of canned food in a 3-D pouch with CFD has been studied by Ghani et al. [6]. CFD for optimization in food processing for optimization in food engineering has been investigated by Erdogdu [8]. Hoang et al. made an analysis of the air flow in a cold store by means of CFD [10].

Understanding the thermal natural convection has become necessary in different branches of science. Remarkably, during the last two decades great interest for food processing applications has awaken [6–9]. With this purpose, numerical analysis and computational fluid dynamic (CFD) software have been used by researchers, coupled with experimental techniques of flow visualization, and temperature measurements [7]. Some of the

CFD applications to simulate convection flow are mentioned as follows. Kumar and Bhattacharya analyzed the convection behavior, temperature change, and also change in airflow of fluid foods during retort sterilization using CFD [12]. The heat transfer in double-sided cooking of meat patties considering two-dimensional geometry and radial 365 shrinkage has been studied by Zorrilla and Singh [13]. The modelling of coupled heat and mass transfer during a contact baking process has been investigated by Feyissa et al. [14]. Gandhi et al. studied the single and two-phase (boiling), natural convection, accompanied by thermal stratification, using CFD simulations and Particle Image Velocimetry (PIV) measurements [7]. The inverse modeling of pan heating in domestic cookers has been performed by Sanz-Serrano et al. [15].

Regarding IH modeling, some studies have been conducted to understand the principles of IH by numerical methods and CFD [16–19]. The numerical analysis of a new coil design for induction heating and its experimental verification with globalization evaluation has been performed by Kang et al. [16]. Huang and Huang studied the effect of multi-layered induction coils on efficiency and uniformity of surface heating, using multiple physical coupling analyses in ANSYS software, to model the thermal effect of induction heating on the surface of the heated target [17]. The numerical optimization for induction heat treatment processes has been analyzed by Naar and Bay [18]. The numerical analysis and thermographic behavior of induction heating, for this purpose they used thermographic cameras in order to validate the temperature distribution and other dynamic changes of a target surface has been investigated by Kranjc et al. [19]. These infrared measurements were obtained based on a color-coded thermal profile, and they demonstrated to be useful tools to control cookware temperature distribution during IH [19].

This manuscript describes the analysis of temperature and the distribution of convection flow of three different cookware materials composed of stainless steel, aluminum and enameled iron, when heating oil in an induction stove. For this purpose, a computational fluid dynamic (CFD) software COMSOL Multiphysics© has been employed, to analyze the heat transfer process. In regard of the type of oil employed in this study, we observed that olive oil maintains most of its nutritional properties during frying of different meals [20] and therefore it has been selected for this study. In addition, a thermographic camera and particle tracer have been used to compare the measurements of temperature, heat transfer, and flow velocity, obtained from the CFD analysis.

2 Materials and experimental method

2.1 Experimental equipment

The cookware was placed on an induction stove; model Mini Small Portable Induction Cooktop stove SC-10B. This model has only one induction zone with a nominal power of 1,000 W, a voltage of 110 V and nine power levels. The procedure of the performed tests consisted in cookware heating with and without olive oil, within laboratory conditions of 15 °C and 70 % of humidity. In order to measure the temperatures on the base as well as on the sides of the cookware, it used a thermographic camera, model FLUKE Ti125 that records temperatures from –30 °C to 385 °C.

The cookware has been manufactured by UMCO, which is the biggest cookware industry in Ecuador. The main characteristics of the cookware used in the tests are presented in Table 1. The thermophysical properties of the cookware have been given by UMCO which tested them in the laboratories of Polytechnic National University of Quito [4, 21]. The first cookware that was tested in this study is made out of enameled iron in its body and bottom; the second cookware is made of AISI 304 stainless steel in its body and a three layer material made of AISI 430 stainless steel, aluminum and iron in its base, all of them weld together to the body. All lids are made of AISI 430 stainless steel layer. The body of the third cookware tested, is made of aluminum, and the bottom of AISI 430 stainless steel. Hereafter the cookware will be referred to as enameled iron, stainless steel and aluminum.

For these tests the cookware had different thickness. It is due that the enameled iron and stainless steel cookware would weigh too much if they had the same thickness as the aluminum pot. In the case of aluminum cookware, these would present problems in the mechanical strength if they had the same thickness as the enameled iron and stainless steel cookware [4, 22–24]. For this reason they have not been found cookware that have the same thickness at its base with different cookware materials and it has been tested the commercial cookware most similar in their geometrical characteristics.

Table 1: Geometrical and thermal characteristics of tested cookware.

N°	Material of the body	Material of the bottom	Diameter of the bottom [m]	Diameter of the top [m]	Thickness of the body [m]	Thickness of bottom [m]	Height of the cookware [m]	Thermal conductivity of BM $[\frac{W}{m \times K}]$	Specific heat of the body $[\frac{J}{kg \times K}]$	Density $[kg/m^3]$	Thermal Diffusivity $*10^{-5}$ $[\frac{m^2}{s}]$
1	Enameled iron	Enameled iron	0.16	0.20	0.0010	0.0010	0.07	53.3	500	7,180	1.48
2	AISI 304 Stainless steel	AISI 430 Stainless steel	0.17	0.20	0.0012	0.0018	0.08	24.9	505	7,800	0.63
3	Aluminum	AISI 430 Stainless steel	0.14	0.20	0.0020	0.0025	0.08	20.9	909	2,700	0.85

2.2 Olive oil temperature and heat flux distribution measurements on the cookware

In order to measure the oil temperature on the cookware during the IH, a K-type thermocouple of 1 mm in diameter joined to a Fluke Multimeter 289 was used. The thermocouple endings have been submerged in the olive oil and placed at the center, half and border of the bottom. A volume of 0.5 L to perform the oil heating process was used for the study. The temperature and pressure never reached the boiling point during the test, so as to analyze the heating speed in each cookware and the natural convection of the oil distribution. The complex behavior of the oil phase changes has not been considered, to simplify the heat transfer model of the oil to a natural convection transfer process.

The surface temperature of the oil has been measured with an infrared thermometer, model W/ Laser Mastercool World Class Quality, 52224-A. Furthermore, two thermographic cameras model FLUKE Ti125 have been set, one of them in the front of the cookware with a separation of 1.00 m. The second camera was set perpendicular at the base of the cookware with a separation of 1.20 m. To achieve adequate temperature measures, the thermographic cameras were set with an emissivity of 0.9, and at the same time these temperature measures were contrasted with the infrared thermometer described earlier. Then, the induction stove was turned on at the same time the thermographic cameras started recording the outstanding temperature variations in a video, for this study. The cameras were able to record the thermographs of the bottom and lateral sides of the cookware at different times, which has allowed tagging the temperature distribution for several points of the cookware bottom.

The temperature analysis of the thermographic images at the sides and the bottom of the cookware were performed during the heating and cooling process. Values of temperatures were obtained every second; in the case of measuring the cookware without fluids, the measurements were taken during five minutes, or until the temperature sensor of the thermographic camera reached its limit of 385 °C. In the case of measuring the cookware with fluids, the measurements were recorded until the boiling point was reached.

The electromagnetic field analysis has been modeled using the COMSOL Multiphysics© software, in order to obtain the heat distribution at the bottom of the cookware. To model the heat generation distribution in the cookware, a three-dimensional finite element model has been developed using the characteristics and properties of the induction stove and the cookware materials. To simulate the electromagnetic field, a multi-turn coil from plane copper coil, consisting of 22 wires of electrolytic copper and 0.5 mm of diameter was employed. The materials and geometry of the coil was modeled in function of the datasheet of the stove used in the test [6]. The temperature distribution and convection velocity have been calculated joining the two Multiphysics modules at the same time [25, 26].

Once the heating test was finished, the stove was turned off and the temperature during the cookware cooling period was measured. Measures were taken until the cookware central zone reached a temperature of 65 °C in the case of cookware without oil, and during five minutes in the case of cookware with oil. The analyzed points were used to plot graphs of temperature against time. The obtained temperature data were used to make a CFD analysis, in order to obtain results related with convective heat flux, through the modulation and simulation with the COMSOL Multiphysics© software.

2.3 Visualization of convection flow in the cookware

Particle tracers have been used for the visualization of olive oil flow in the cookware by imitating the method for olive oil particle tracers [, [2]. The particle tracer density has been well-adjusted to the density of the olive oil (970 kg/m^3). The particle tracer measured 0.0015 m of diameter. The tracer solution was exactly balanced to 5.8 % isobutyl isopropyl ether quantity.

2.4 Physical model

The cookware dimensions for the analytical model had 0.045 m in height, and had different diameters as presented in Table 1. The volume of olive oil considered in the cookware was equal to 0.5 L. To simulate the same conditions for this volume in the experiment, the height of the olive oil on the cookware was 0.044 m. The thermophysical properties of the olive oil as a function of the temperature are presented in Table 2 for the simulation. The initial temperature was assumed as T_{outdor} = 15 °C to start the simulation.

Table 2: Thermophysical properties considered by the olive oil [11].

Description	Units	Equation
Density	**kg/m³**	$\rho = 1098.29 - 0.60T - 1.55 \times 10^{-05}T^2$
Dynamic viscosity	**Pa s**	$\eta = 117015.2{-}1844.98T + 11.64T^2 - 0.0367T^3 + 5.806 \times 10^{-05}T^4$ $-3.67 \times 10^{-8}T^5$
Thermal expansion	**1/K**	$\alpha = 1.98 \times 10^{-04} + 6.08 \times 10^{-08}T + 7.04 \times 10^{-11}T^2$
Thermal conductivity	**W/(m*K)**	0.169 from 283 °K to 372 °K
Specific heat	**J/(kg*K)**	1,999.477

2.5 Assumptions

In order to simplify the problem, the following assumptions have been made:

1. Axi-symmetry: The cookware shape has been assumed as a cylinder. For this reason, the convection flow shows axial symmetry due to the axi-symmetrical heating conditions.
2. The heat generation due to viscous dissipation is negligible.
3. The Boussinesq approximation has been applied for the buoyancy effect.
4. No-slip conditions have been assumed at the inside cookware wall.
5. Natural convection is assumed during the simulation, in as much as it was performed below the olive oil boiling point. During the simulation laminar flow is conducted due to the Rayleigh number $<10^9$.
6. The gravity force of 9.8 m/s^2 has been introduced axially to the cookware.

2.6 Model equations

2.6.1 Analysis of electromagnetic field

The electromagnetic model was based on Maxwell equations. These equations allow the calculation of heat through the base of the cookware with the electromagnetic field generated by the coil; which is the input to solve the heat transfer equation as well as the fluid flow equation. The heat generated in the cookware depends on three principal factors that are: the electric current density, the distance between cookware and coil and the number of loops of the coil. This system is based on the four following equations to calculate the effect of electromagnetic field:

- Magnetic flux

$$\nabla . B = 0 \tag{1}$$

- Maxwell – Gauss

$$\nabla . E = 0 \tag{2}$$

- Maxwell – Faraday

$$\vec{\nabla} x \, \vec{E} = -\frac{\vec{B}}{t} \tag{3}$$

- Maxwell – Ampere

$$\vec{\nabla} x \, \vec{H} = \vec{J} + \frac{\vec{D}}{t} \tag{4}$$

To obtain a closed system, the equations include constitutive relations that describe the macroscopic properties of the medium. They are given as:

$$\mathrm{D} = \varepsilon_o \varepsilon_r E \tag{5}$$

$$\mathrm{B} = \mu_o \mu_r H \tag{6}$$

$$\mathrm{J} = \sigma E + J_e \tag{7}$$

The equations can be formulated in differential form or integral form. The differential form is presented here because it leads to differential equations that the finite element method can handle. For general time-varying fields, Maxwell and Ampere's law equation can be written in function of constitutive relations as:

$$\left(jw\sigma - w^2 \varepsilon_o \varepsilon_r\right) + \nabla \mathrm{X} \left(\mu_o^{-1} \mu_r^{-1} B\right) - \sigma \mathrm{v} X B = J_e \tag{8}$$

A Multi-Turn coil boundary condition was used in order to simulate the magnetic field, which is generated by electric currents.

$$J_e = \frac{N I_{coil}}{A} \tag{9}$$

2.6.2 Analysis of conjugate heat transfer

This model involved the incompressible Navier-Stokes equations from fluid dynamics with a heat transfer equation. For this model, there were four unknown field variables (dependent variables):

The incompressible Navier-Stokes equations consist of a momentum balance (a vector equation), a mass conservation (10), and an incompressibility condition (11):

$$\rho \frac{u}{t} + \rho u \cdot \nabla u = -\nabla p + \eta \nabla^2 u + F \tag{10}$$

$$\nabla \cdot u = 0 \tag{11}$$

The heat equation is an energy conservation equation that exposes that the change in energy is equal to the heat source minus the divergence of the diffusive heat flux (12):

$$\rho C_p \left(\frac{T}{t} + u \cdot \nabla T\right) + \nabla \cdot (-k \nabla T) = Q \tag{12}$$

2.7 Boundary conditions

The boundary conditions to solve the physical model were:

(a) Thermal insulation in the bottom because the cookware bottom was in contact with the vitroceramic material of the stove, which has a low conductivity capacity. For this reason, the heat loss through vitroceramic was negligible.

(b) Use of convection heat flux boundary condition driven by the temperature difference between the sides of the cookware wall and the surrounding atmosphere.

(c) Use of convective heat flux boundary condition driven by the temperature difference between the cookware and the olive oil. In the internal wall the flow speed was 0, and in the external wall there was heat transfer between the inside cookware and environment.

(d) The heat flux generated within the cookware bottom was set to 1,000 W which is the power calculated in the induction heating analysis.

Boundary conditions for the cookware surface: (r = R, z = 0) were: $v_r = 0$; $v_\theta = 0$; $v_z = 0$

Olive oil temperature and initial velocity conditions were: $T = T_{ref} = 15$ °C;

$v_r = 0$; $v_\theta = 0$; $v_z = 0$ at $0 \leq r \leq R$, $0 \leq h \leq H$

(e) Volume force was used to simulate the effect of natural ventilation in olive oil. It was changing during the heating process.

$$F = -g * \rho\,(T, t) \tag{13}$$

2.8 Solution strategy

The convection flow of the olive oil in the cookware during IH has been simulated by COMSOL Multiphysics© software which is based on the finite elements method. For this purpose, the axi-symmetry and the calculation for only half of the cookware has been taken into account. However, when convection occurred in the oil and air, the calculation has been complex and lasted longer.

CFD was customized by COMSOL Multiphysics© programming to introduce the heat generation into the CFD calculation by induced Eddy-current losses, or so called skin effect. The high-frequency current or the electromagnetic field is limited to the surface of the conductor. The measurements of the different cookware have been assumed.

The generated heat flux and temperature distributions within the bottom and in the axial direction of the cookware was determined by the electromagnetic field analysis (EFA), for the three different cookware materials as listed in Figure 1. Their values were used for the CFD analysis by the COMSOL Multiphysics© module. In the case of the enameled iron and the stainless steel, we observed that the heat distribution is similar and decreased in the center and the side of the cookware.

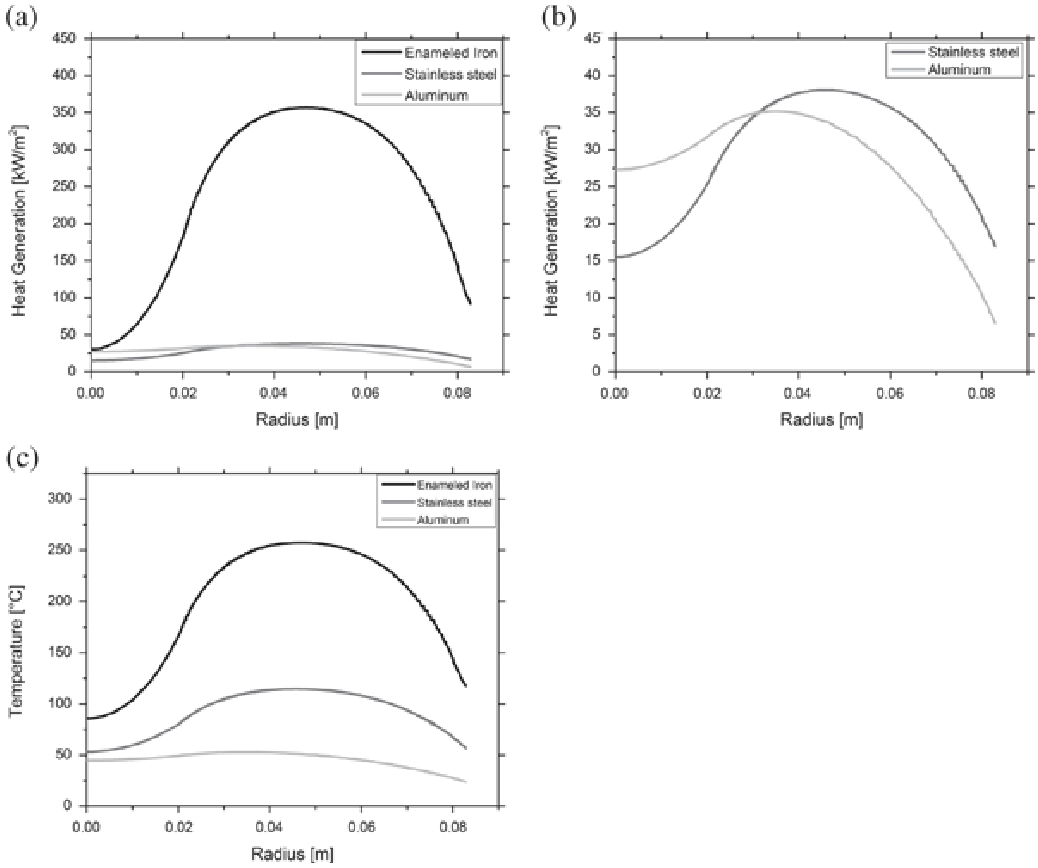

Figure 1: Generated heat flux distribution within the bottom of the cookware, with its body made of (a) enameled iron, stainless steel, aluminum; where 0, on the horizontal axis, is the center of the cookware. (b) Detail of the heat flux distribution for stainless steel, aluminum. (c) Temperature distribution within the bottom of the cookware. The results have been determined by EFA.

The heat distribution decreases when getting close to the center and close to the side of the cookware, like a doughnut shape. Meanwhile in the case of the aluminum body cookware, the heat distribution decreases only when getting close to the lateral sides of the cookware. In the case of the enameled iron cookware, the maximum value of heat flux detected reached 365,000 W/m^2, at 0.0475 m of the radius with respect to the center of the cookware. The stainless steel cookware reached the highest values of heat flux of the three compared cookware materials. In this material, the heat flux achieved 38,500 W/m^2 at 0.0475 m of the radius with respect to the center of the cookware. Whereas, the aluminum body cookware presented maximum value of heat flux that reached 35,000 W/m^2, at 0.035 m of the radius, with respect to the center of the cookware.

The cookware thickness is an important parameter to be considered when analyzing the heat distribution in the cookware bottom [28, 29]. This parameter influences directly over the induced current which is not uniform along the cookware bottom. As much as the thickness increases, the current density decreases. Therefore, the thickness of skin effect depends of induction frequency generated by the coil of the induction stove as well as the electrical material properties like resistivity and permeability. In this layer 87 % of the total power has dissipated by the induction cooker. Thus, we can say that the heat transfer is generated in this zone.

In this context, the enameled iron cookware as shown in Figure 1(c) has the highest temperature distribution. This cookware has the least skin depth (0.04 mm) of all three cookware that were analyzed. The cookware materials with aluminum and stainless steel have the highest skin depth with 1 mm.

2.9 Computational Grid

To solve the differential equations used in the physical model, a free triangular mesh with extra-fine resolution was built to ensure the model convergence as it can be observed in Table 3. The P2+P1 numerical discretization method is used, where the first number is the element order for the fluid velocity, and the second number is the element order for the pressure. The convergence criteria used in the simulation has two steps:

(a) When the simulation started, a slight period of time was chosen, in order to solve the model. Then, if the solution did not converge, it kept varying the time period until the solution converged and the period of time was constant.

(b) When the error was close to zero and it was constant during the simulation.

Table 3: Mesh element size parameters.

Element size parameters	
Maximum element size	0.0017 m
Minimum element size	6.38×10^{-06} m
Maximum element growth	1.2
Resolution of curvature	0.25
Resolution of narrow regions	1

The computational model to calculate the natural convection of olive oil heating has been conducted for 400 s. The interval of time for each result was 0.01 s. For this purpose, 40,000 steps were necessary. This computational model has required 18 h of cluster time on the ENSIMS X3200 cluster of Dell Power Edge T620 (two CPUs speed 2.7 GHz), a RAM of 64 GB and a 24 processor core.

3 Results and discussion

3.1 Observation of temperature distribution with radiation thermometer

The visualization of temperature distribution by thermographic images of the cookware heated on the surface by IH after 15 s, for empty cookware, is shown in Figure 2. We observed that in the enameled iron, the bottom of the cookware was heated in a doughnut shape, just above the coil (Figure 2(a)). This heated part rose to the highest temperature. In the case of the stainless steel and aluminum cookware, the distribution of temperatures is similar in all two bases (Figure 2(b) and Figure 2(c)). These results indicated that the higher heating temperature for the inner base of enameled iron, with the same power selected of the cooker should be correlated with a higher energy efficiency of the system cooker-cookware. For the side of all three cookware, we observed that the bottom acquired a higher temperature, because the cookware was empty (Figure 2(d) and Figure 2(f)). In the case of the enameled iron and aluminum cookware, a hot zone due to high permeability of the first one and the heat conductivity of the second one has been observed (Figure 2(f)). However, in the case of stainless steel the smallest hot zone has been detected, due to the lower heat conductivity in comparison to the aluminum material (Figure 2(e)).

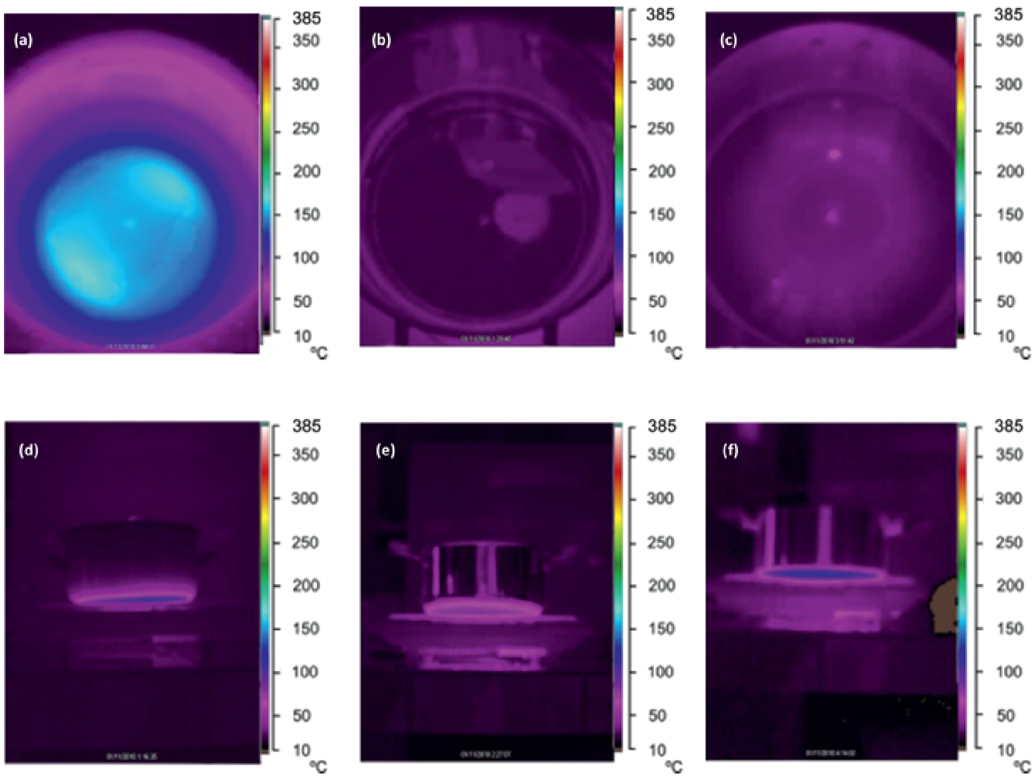

Figure 2: Temperature distribution by a thermographic camera, images of the cookware heated on the surface by IH after 15 s, for tan empty cookware. Top view and side view for (a), (d) enameled iron, (b), (e) stainless steel, (c), (f) aluminum.

3.2 Heat flux measurements

The heat flux images from the cookware bottom with its body made of enameled iron, stainless steel and aluminum, during the heating process at 15 s, 30 s and 50 s are presented in Figure 3. When the temperature (Figure 2) and heat flux distributions (Figure 3) are compared a similitude between the results is revealed, and the boundary conditions in the case of IH are validated, which are directly related to the natural flow distributions. Results in Figure 3(a) confirmed those results presented in Figure 2(a), that are in relation to the doughnut shape for the temperature distribution of the enameled iron bottom cookware under IH, when the heating time has been increased. A similar behavior appears in Figure 3(b), Figure 3(c) for stainless steel and aluminum body cookware at 50 s of the heating time.

The heat transfer occurs in the contact area between the coil and the cookware bottom surface, since this area is a small part of the whole area, a lot of power is required to extend the heat to the entire area. For this reason, ferrite materials are commonly used for their thermophysical properties. They are required to produce an influence into the magnetic field concentration when given areas thereby refine the heat pattern produced. Emphasizing these obtained results with an empty and with oil filled cookware. In this case, the fluid changed the distribution of temperatures above the base.

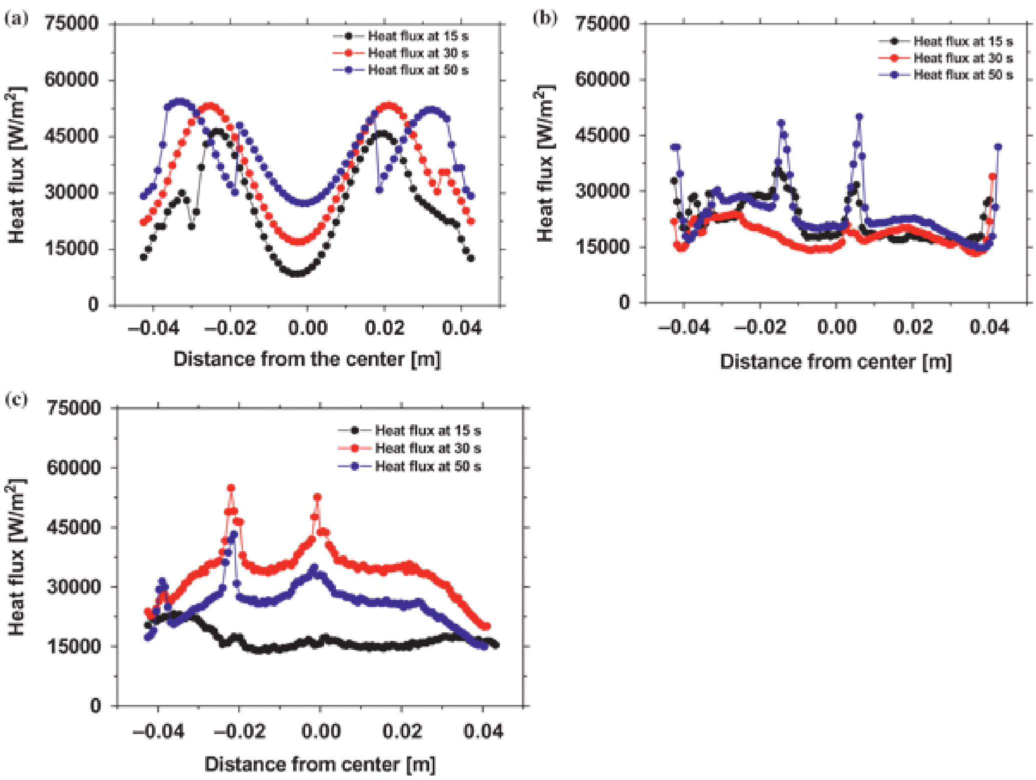

Figure 3: Heat flux results for the cookware bottom with its body made of (a) enameled iron, (b) stainless steel, (c) aluminum, during the heating process at 15 s, 30 s and 50 s.

In the case of the enameled iron cookware, the heat flux achieved a value of 54,000 W/m^2 at 0.033 m from the center of the cookware and in 50 s of the heating process. Meanwhile in the center of the cookware 27,500 W/m^2 were achieved at the same time of the process (Figure 3(a)). For the stainless steel cookware the heat flux achieved a peak value of 50,500 W/m^2 at 0.007 m, from the center of the cookware and in 50 s of the heating process. In the center of the cookware the stainless steel material achieved 20,500 W/m^2 at 50 s of the heating process (Figure 3(b)). The stainless steel cookware the heat flux partially presented higher values on left side than the right side of the Figure 3(b). It is due to the different configurations of the material after machining presenting utensils [21]. The aluminum body cookware heat flux achieved a peak value of 55,500 W/m^2 at 0.022 m from the center of the cookware in 50 s of the heating process, meanwhile achieving 37,500 W/m^2 in the center of the cookware at the same time of the process (Figure 3(c)).

The images of Figure 3 show as the heat flux incremented until a certain temperature and time when it has been stabilized and it started to decreases. Kawakami et al. measured that the heat flow started to decrease after the first 30 s of heating [2].

The distributions showed in Figure 3 depend on the thermal and magnetic material properties of each cookware, as well as the material has a strong relationship with the electromagnetic field generated in the base of the cookware. Although the same electromagnetic field was applied to each cookware, the enameled iron material was heated faster than the others, due to the materials higher thermal conductivity, which is how easily the material absorbs and transmits energy.

Similar results have been reported by Kawakami et al. [2] that are related with the induced Eddy-currents losses, or so-called skin effect. The thermophysical properties such as magnetic permeability and thermal conductivity have influence too. Magnetic permeability has an influence into the magnetic field concentration and thermal conductivity of the material that also has an influence into the conduction heat through the material (Table 1). In the case of stainless steel and aluminum cookware, heat flux and temperature distribution are similar in the base due to the shape of the coils and the stationary induction effect [2].

3.3 Comparison between measured and calculated fluid temperature distribution in the cookware

The contrast between the calculated temperature by COMSOL Multiphysics© and the measured temperature in the border, half and center of the bottom for a stainless steel cookware with 0.5 L of olive oil, measured by the thermographic camera is presented in Figure 4. As shown in Figure 2(a–c), the temperature along the base of the cookware was almost constant. Moreover, after 100 s of heating, an in-homogeneous distribution of the convection may be happen in both cases. This irregular behavior could explain the higher differences between the calculated and measured temperature change of the fluid in the pan presented in Figure 4. Differences have been observed between the COMSOL Multiphysics© and measured temperatures at the initial stage, meanwhile, after 125 s, there was a correlation between the temperature rate for COMSOL Multiphysics© and the experimental measurements.

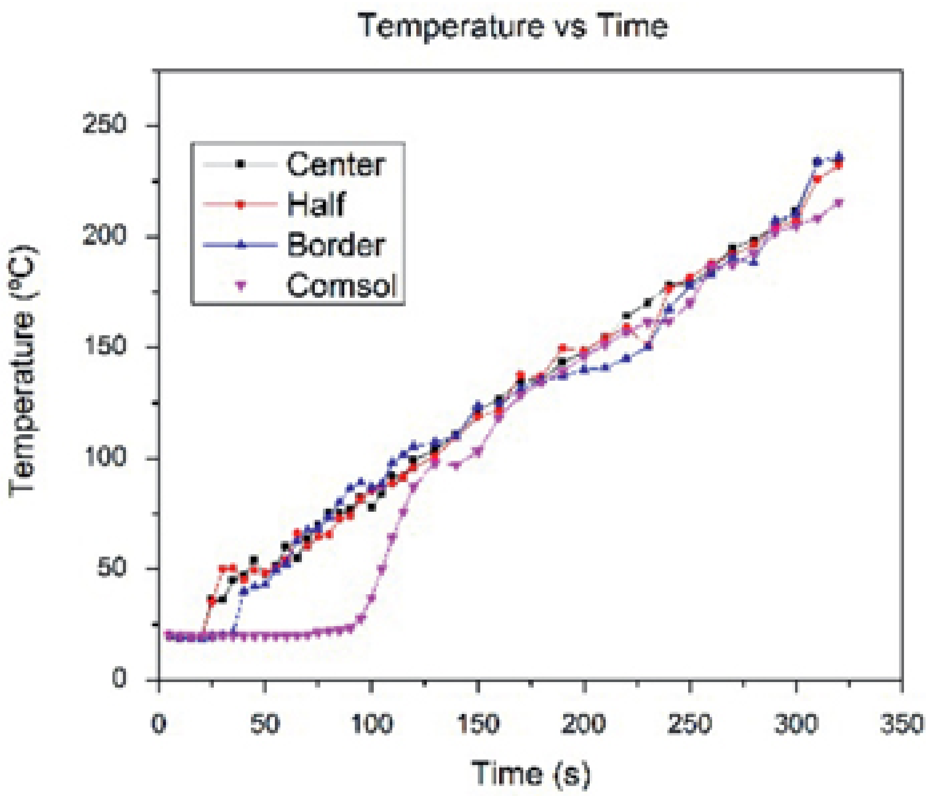

Figure 4: Contrast between the calculated temperature by COMSOL Multiphysics© and the measured temperature in the border, half and center of the bottom for a stainless steel cookware with 0.5 L of olive oil measured by the thermographic camera.

3.4 Visualization of olive oil temperature distribution on the cookware

The olive oil temperature distribution in the cookware heated for 300 s of all three cookware compositions are presented in Figure 5. As soon as the cookware was heated by IH, an increment in the temperature at the bottom of the cookware could be detected. The oil was heated along with the heating of the cookware bottom. In this case, part of the heated oil was rising until reaching the top oil surface after 300 s (Figure 5). In contrast of the cookware bottom visualization, without fluid (Figure 2), we observed that the temperature is homogeneous in the cookware bottom (Figure 5). In the case of enameled iron and the aluminum body cookware, the side temperatures did not rise significantly. While the stainless steel cookware presented the opposite behavior, since the sides of the cookware reached 170 °C at 0.04 m of height for the simulated heating time (Figure 5). The enameled iron, stainless steel and aluminum body cookware materials reached the highest temperature of about 257.8 °C. In the case of the enameled iron and aluminum body cookware the biggest contrails of hotter fluid have been observed going from the bottom to the top (Figure 5 (a and c)). This is due to their thermal and magnetic material properties such as magnetic permeability, specific heat and thermal conductivity. In case of enameled iron (Figure 5(a)) demonstrates how the density of contrails increased in the center of the cookware, and although these contrails were fewer, they were the biggest ones. In the case of the stainless steel cookware (Figure 5(c)), the highest number of contrails going to the top and dispersed by all the bottom area appear, but the contrails and the temperature of the fluid are lower than in the case of enameled iron and the aluminum body cookware.

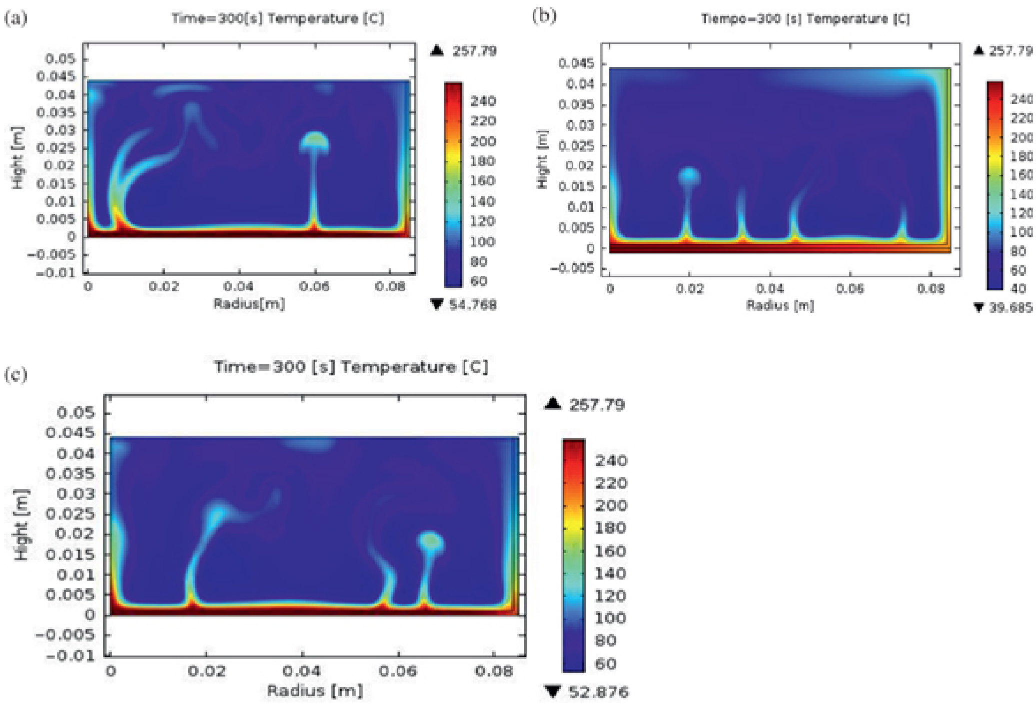

Figure 5: (a) Olive oil temperature distribution in the cookware heated vs height and radius in 300 s for (a) enameled iron, (b) stainless steel and (c) aluminum. The right extremity of the images is the side of the cookware, and the left extremity of the images is the center of the cookware.

In addition, it has become clear that the oil near the bottom of the cookware received higher IH in enameled iron and aluminum body cookware. It was due to their high magnetic permeability and thermal conductivity, and the highest thermal diffusivity. Thermal diffusivity is a property that indicates how fast the heat would be transferred through and out of the material. Thermal diffusivity is the thermal conductivity divided by the heat capacity unit (Table 1). Meanwhile, the liquid of the top was at the lowest temperature. It created a buoyancy force due to the change in the density of the oil by different temperatures, which generated a rising flow, from the bottom to the top of the cookware. The buoyancy-driven flow induces recirculation zones in the oil. Therefore, the flow going up is turned to the radially direction to the side of the cookware. In this position, the oil gets a lower temperature and becomes heavier, which produces a downfall movement close to the bottom surface near to the coil, which generates the movement again.

3.5 Comparison between measured and calculated olive oil convection flow distribution on the cookware

The visualization of the convection flow with tracer particles in the initial stage of IH for enameled iron, stainless steel and aluminum are presented in Figure 6. The images have been taken with a camera above the cookware every 2 s. We observed that the particles moved from the center towards the outside wall of the cookware. The average speed v of the tracer particles was calculated using $v = \sqrt{v_x^2 + v_y^2 + v_z^2}$. Flow velocity at the early stage and after 300 s of heating, for the different cookware are detailed in Table 4. We detected that enameled iron cookware has the highest results of flow velocity at the early stage and after 300 s of heating. Furthermore, aluminum body cookware presented the best results of flow velocity than the stainless steel cookware.

The authors detected some errors by comparing the measured velocity to the modeled velocity. The average relative error for enameled iron was 35 %, 31 % for stainless steel and 29 % for aluminum cookware. Some of the reported literature on CFD is in the percentage line of these errors. Kawakami et al. measured 33 % of error to predict the boiling water, and [2] reported an error range of 26–28.5 %, in order to simulate the airflow pattern in a cold store. Mirade and Daudin [11] presented an error of 40 % when they studied the air flow pattern in a chiller with objects.

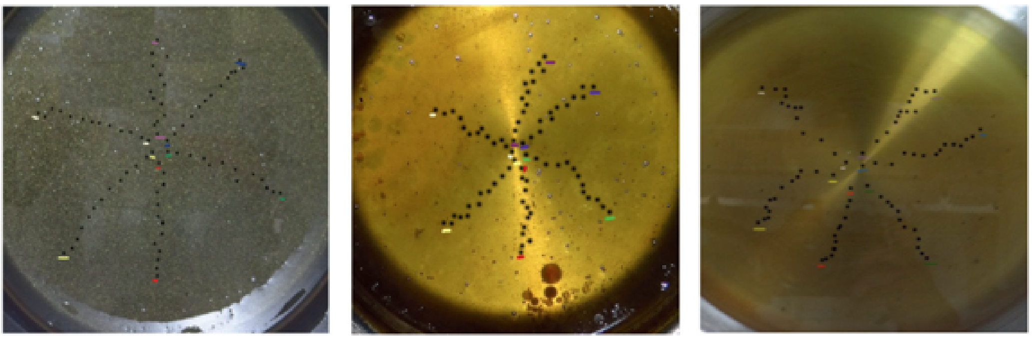

Figure 6: Visualization of the convection flow with tracer particles in the initial stage of IH for (a) enameled iron, (b) stainless steel, (c) aluminum. The tracer particles moved from color lines which are at a start and an end position. Images were overwritten every 2 s from 5 to 31 s of heating.

Table 4: Flow velocity at the early stage and after 300 s of heating for enameled iron, stainless steel and aluminum body cookware.

	Early stage of heating			At 300 s of heating		
	enameled iron	stainless steel	aluminum	enameled iron	stainless steel	aluminum
Flow velocity (m/s)×10^{-6}	5.4	4.2	4.8	2,321	1,027	2,115

The convection flow calculated with COMSOL Multiphysics© for the different cookware materials heated by IH after 10, 60 and 300 s are presented in Figure 7. To compare the changes in the convection flow for each time, it has kept the scales of the Figure 7 x.1 for all images to 10 s, for Figure 7 x.2 for all images to 60 s and for Figure 7 x.3 for all images to 300 s. A correlation between the experimental measurements and the COMSOL Multiphysics© values has been detected. The length of the arrow and the color of the scale showed the magnitude of natural convection flow, while the scale of the images and the direction of the arrow showed the direction of the convection. While the convection had barely occurred at 10 s of the heating process, after 60 s the convection raised from the base and the side of the cookware, especially in stainless steel as can be observed in Figure 7(b.2)). After 300 s the different patterns of the natural convection flow can be observed. In the case of the enameled iron (Figure 7(a.3)) the biggest contrails and natural convection flow in the middle of the cookware can be detected. The tendency of convection from the inside to the outside was strengthened after 300 s of heating. This is due to the thermophysical properties such as high magnetic permeability, thermal conductivity and thermal diffusivity. For the stainless steel (Figure 7(b.3)) the lowest contrails and natural convection flow was observed. Whereas, at the aluminum body cookware (Figure 7(c.3)) the contrails of the natural convection flow dispersed by the oil into the cookware were clear for the viewers.

(c.1)

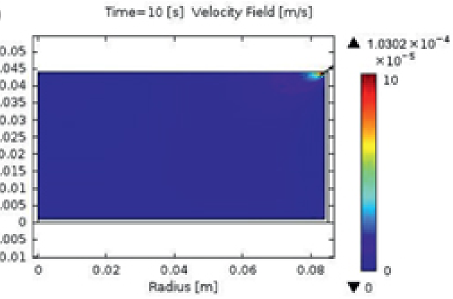

(c.2)

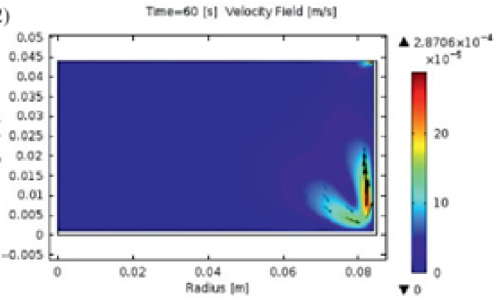

(c.3)

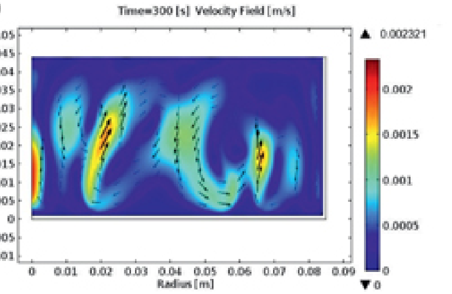

(c.1)

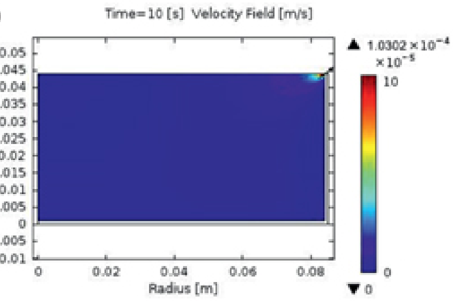

(c.2)

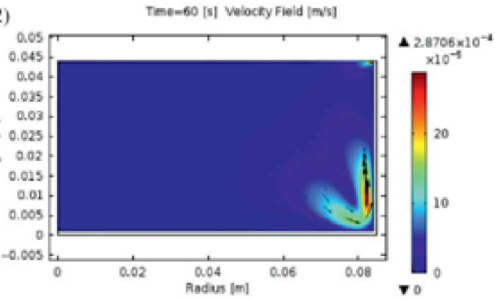

(c.3)

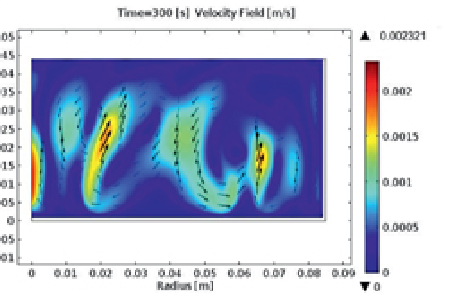

(c.1)

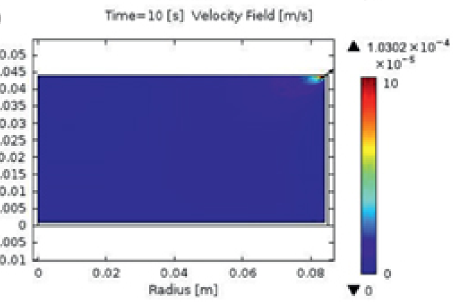

(c.2)

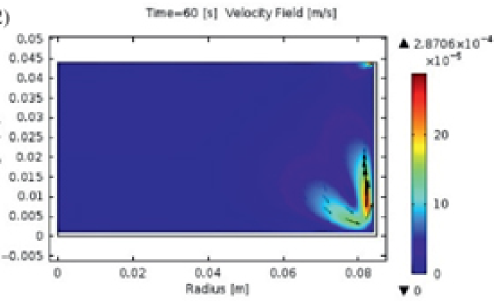

(c.3)

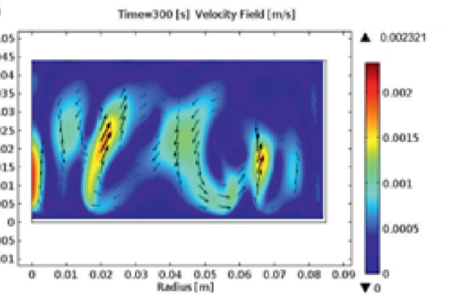

Figure 7: Calculated natural convection flow in the cookware of (a) enameled iron, (b) stainless steel and (c) aluminum after 10, 60 and 300 s. The right extremity of the figure is the side of the cookware, and the left extremity of the figure is the center of the cookware.

4 Conclusions

The performance of convection flow and temperature in different induction cookware compositions such as stainless steel, aluminum and enameled iron during boiling olive oil have been analyzed using COMSOL Multiphysics©. The results showed that COMSOL Multiphysics© can accomplish the estimation of the convection flow of olive oil heated in the cookware by IH. In addition, in order to compare the results of temperature, heat transfer and flow velocity obtained from CFD analysis, experimental measurements of a thermographic camera and a particle tracer have been performed as well.

The increment of the temperature rate in the experimental results correspond with the one calculated by CFD. The biggest contrails of hotter fluid going from the bottom to the top have been detected in the enameled iron and aluminum cookware. At the enameled iron cookware material the density of contrails increased around the midpoint of the cookware. In the case of stainless steel, the temperature of the fluid is lower than temperatures of the other two cookware materials, but the number of contrails is higher.

While the convection had scarcely occurred at 10 s of heating, the convection increased from the base and the lateral of the cookware after 60 s. Clearly different patterns of convection flow velocity were observed after 300 s. At this time, the enameled iron presented the biggest contrails and convection flow velocity in the middle of the cookware. This reason and the increment of the temperature of the fluid make the enameled iron the best choice for cookware material in induction stoves.

Magnetic permeability and thermal diffusivity are decisive for the choice the distribution of material for the base of the pots. Magnetic permeability has influence into the magnetic field concentration in the base of the cookware. Thermal diffusivity contributed in how fast the heat would be transferred through and out of the material.

To conclude, this study contributes to the literature about CFD analysis and comparisons with experimental models in fluids. This research helps to understand the thermal natural convection of olive oil. It is the first research to evaluate the most suitable constitution of cookware materials for induction stoves.

For future work, we recommend to perform the same analysis presented in this work, but making a comparison between cookware of the same dimensions. It is responsibility of the cookware producers to consider manufacturing cookware with similar dimensions that the ones that are currently in the market.

Nomenclature

Nomenclature		Nomenclature	
u	**velocity of the field**	$\vec{H}$	**magnetic field (A/m)**
p	**pressure (N/m^2)**	$\vec{J}$	**electric current density (A/m^2)**
F	**volume Force**	t	**time (s)**
ρ	**density of the fluid (kg/m^3)**	T	**temperature (°C)**
η	**dynamic viscosity**	$\vec{B}$	**magnetic induction (N s/C m)**
∇	**vector differential operator**	$\vec{D}$	**electric flux density (C/m^2)**
$\vec{A}$	**magnetic vector potential (V s/m)**	$\vec{E}$	**electric field (V/m)**
C_p	**heat capacity of the fluid**	Q	**source term**
ε_o	**permittivity of vacuum**	μ_o	**permeability of vacuum**
σ	**electrical conductivity**	**N**	**number of turns of the coil**
A	**total cross area of the coil**	I_{coil}	**total current**
u	**velocity field component in axis x**	v	**velocity field component in axis y**

References

1. Wong KK. Experimental study of induction cooker fire hazard. Procedia Eng 2013;52:13–22.
2. Kawakami H, Llave Y, Fukuoka M, Sakai N.. CFD analysis of the convection flow in the pan during induction heating and gas range heating. J Food Eng 2013;116(3):726–736.
3. Sung YT, Hwang SJ, Lee HH, Huang DY. Study on induction heating coil for uniform mold cavity surface heating. Adv Mech Eng 2014;6:349078.
4. Villacís S, Martínez J, Riofrío AJ, Carrión DF. Energy efficiency analysis of different materials for cookware commonly used in induction cookers. Energy Procedia 2015;75:25–930.
5. Martínez-Gómez J, Ibarra D, Villacis S, Cuji P, Cruz PR. Analysis of LPG, electric and induction cookers during cooking typical Ecuadorian dishes into the national efficient cooking program. Food Policy 2016;59:88–102.
6. Ghani AGA, Farid MM, Chen XD, Richards P.. Thermal sterilization of canned food in a 3-D pouch using computational fluid dynamics. J Food Eng 2001;48:147–156.
7. Gandhi MS, Sathe MJ, Joshi JB, Vijayan PK. Two phase natural convection: CFD simulations and PIV measurement. Chem Eng Sci 2011;66:3152–3171.
8. Erdogdu F.. Computational fluid dynamics for optimization in food processing. Erdogdu F, editors. Optimization in Food Engineering. Boca Raton, FL: CRC Press Taylor & Francis Group, 2009:219–227.
9. Farinu A.. Heat and mass transfer analogy under turbulent conditions of fryingUniversity of Saskatchewam Saskatoon, 2001.
10. Hoang ML, Verbonen P, De Baerdemaeker J, Nicolaï BM. Analysis of the air flow in a cold store by means of computational fluid dynamics. Int J Refrig 2000;23:127–140.
11. Mirade PS, Daudin JD. Numerical simulation and validation of the air velocity field in a meat chiller. Int J Appl Sci Comput 1998;5(1):11–24.
12. Kumar A, Bhattacharya M.. Transient temperature and velocity profiles in a canned non-Newtonian liquid food during sterilization in a still-cook retort. Int J Heat Mass Transfer 1991;34:1083–1096.
13. Zorrilla SE, Singh RP. Heat transfer in double-sided cooking of meat patties considering two-dimensional geometry and radial 365 shrinkage. J Food Eng 2003;57:57–65.
14. Feyissa AH, Gernaey KV, Ashokkumar S, Adler-Nissen J.. Modelling of coupled heat and mass transfer during a contact baking process. J Food Eng 2011;106:228–235.
15. Sanz-Serrano F, Sagues C, Llorente S.. Inverse modeling of pan heating in domestic cookers. Appl Thermal Eng 2016;92:137–148.
16. Kang CG, Seo PK, Jung HK. Numerical analysis by new proposed coil design method in induction heating process for semi-solid forming and its experimental verification with globalization evaluation. Mater Sci Eng 2003;341(1):121–138.
17. Huang MS, Huang YL. Effect of multi-layered induction coils on efficiency and uniformity of surface heating. Int J Heat Mass Transfer 2010;53(11):2414–2423.
18. Naar R, Bay F.. Numerical optimization for induction heat treatment processes. Appl Math Model 2013;37(4):2074–2085.
19. Kranjc M, Zupanic A, Miklavcic D, Jarm T.. Numerical analysis and thermographic investigation of induction heating. Int J Heat Mass Transfer 2010;53:3585–3591.
20. Allouche Y, Jiménez A, Gaforio JJ, Uceda M, Beltrán G.. How heating affects extra virgin olive oil quality indexes and chemical composition. J Agric Food Chem 2007;55(23):9646–9654.
21. Orozco M, Martínez J, Riofrío A, Vaca D, Carrión D.. Estudio de ensayos de eficiencia energética, concavidad, convexidad y rugosidad en menaje para cocinas de inducción. Memorias del Congreso latinoamericano de ingeniería mecánica COLIM 2014;8:255–61.
22. Chauhan A, Vaish R.. Magnetic material selection using multiple attribute decision making approach. Mater Des 2012;36:1–5.
23. Callister WD, Rethwisch DG.. Materials science and engineering: an introduction Vol. 7. New York: Wiley, 2007:665–715.
24. Martínez J.. A multi-criteria decision analysis (MCDA) for materials selection of a magnetic application. J Avances 2015;7(1):C1–C8.
25. Multiphysics, COMSOL. Comsol multiphysics user guide (version 4.3 a) 2012;AB: 1-40.
26. Cai L, White RE.. Mathematical modeling of a lithium ion battery with thermal effects in COMSOL Inc. Multiphysics (MP) software. J Power Sources 2011;196(14):5985–5989.
27. Vazquez N, LLop J. Development of new analogues D2 receptor ligands which incorporate a dicarbacloso dodecaborano unit: Carbon-11 labeling and ex vivo and in vivo. U. Pais Vasco 2012;:1–30.
28. Pan Z, Singh RP, Rumsey TR. Predictive modeling of contact-heating process for cooking a hamburger patty. J Food Eng 2000;46(1):9–19.
29. Sedighi M, Dardashti BN.. Heat transfer modeling in multilayer cookware using finite element method. Int J Sci Eng Investig 2012;1(1):190–196.